IQ Imbalance in Heterodyne Transceivers with zero-second-IF for Wide-Band mmW Links

Ainhoa Rezola*†, Juan Francisco Sevillano*†, Martin Leyh‡, Moises Lorenzo‡, Roc Berenguer*†, Aharon Vargas‡ and Igone Vélez*†

*Electronics and Communications Department,
Centro de Estudios e Investigaciones Técnicas (CEIT), 20018 San Sebastián, SPAIN
Email: {argarciandia,jfsevillano,rberenguer,ivelez}@ceit.es
†Electrical, Electronic and Control Engineering Department,
Technology Campus of University of Navarra (TECNUN), 20018 San Sebastián, SPAIN
‡Fraunhofer Institute for Integrated Circuits (IIS), D-91058 Erlangen, Germany
Email: {martin.leyh,moises.lorenzo,aharon.vargas}@iis.fraunhofer.de

***Abstract*—Millimeter wave links are an attractive solution for mobile network backhaul. In order to cope with the requirements of future networks, these millimeter wave links should achieve Gigabit data rates. These data rates can be achieved by using wide-band and high order modulations in E-Band. Heterodyne architectures are good candidates for integrated transceivers, but, the design of integrated transceivers at these frequencies is a challenging issue. An important source of degradation is I/Q imbalance, which can significantly reduce the performance of a communication system with zero-second-IF transceivers if it is not appropriately compensated. The article analyzes the source of this IQ imbalance and proposes the use of different digital processing techniques, including a linear adaptive equalizer scheme. The performance of the transceiver is analyzed at system level by means of simulations. The results presented in the article suggest that the use of those techniques is able to mitigate the impact of the IQ imbalance effects, in order to allow the use of a high-order modulation such as 64QAM.**

***Index Terms*—Mobile backhaul; millimeter-wave; transceivers; RF impairments.**

I. Introduction

The growing demand for ubiquitous broadband communication, e.g., fourth-generation (4G) wireless, has motivated the deployment of ultra high-speed communication systems. Particularly in backhauling networks, optical fiber is required to transport very high data rates. However, optical fiber exhibits important drawbacks, such as high costs, long deployment times, and low flexibility. Recently, point-to-point wireless communication systems have been proposed as an attractive alternative to optical fiber. In order to achieve data rates that are comparable to optical fiber, these communication systems demand very high bandwidth in order to transport enough data. Although the frequency spectrum is congested, the regulation of the E-band, which is around 80 GHz, facilitates the deployment of high-speed communication systems in which a huge amount of data can be transmitted. The European Telecommunications Standards Institute (ETSI) is carrying out a standardization process for this frequency band [1], [2], [3].

Commercial off-the-shelf communication systems operating in the E-band support data rates of up to 2.5 Gbit/s. However, new applications demand even higher data rates (around 10 Gbits/s), which necessitates both wide-band and high-order modulations to utilize the spectrum efficiently. High bandwidths and higher-order modulation waveforms pose special challenges for communication systems offering reliable links at very high data rates. The digital base-band must be able to encode/decode and modulate/demodulate a huge amount of information while employing high efficiency algorithms to guarantee reliable communications. In addition, analog-to-digital converters (ADCs) and digital-to-analog converters (DACs) must work at very high sampling rates. Furthermore, higher order modulations are desirable to boost up the data rate, requiring higher carrier-to-interference (C/I) ratios at the receiver. This involves carefully analyzing the degradation effects introduced by the analog RF impairments and evaluating the corresponding compensation algorithms in the digital baseband processing [4].

In this article we focus on the IQ imbalance impairment, which is one of the performance-critical effects of interest in zero-second-IF transceiver architectures. This impairment, caused by mismatches in the amplitude and phase responses of the I and Q signal paths, entails a degradation in the Image Rejection Ratio (IRR), which is theoretically infinite and causes interfering images at mirror frequencies. IQ imbalance encountered in narrow-band systems can be regarded as non-frequency-selective (NFS), and it is mainly caused by the local oscillators used for quadrature modulation or demodulation. However, IQ imbalance in wide-band systems may also exhibit frequency-dependent or frequency-selective (FS) behavior due to mismatches between the analog filtering paths of the I and Q components caused by finite tolerances [5] [6].

The article analyzes the impact of both non-frequency-selective and frequency-selective imbalances in the transmitted and received signal. In addition, different options for mitigating the NFS and FS IQ imbalance are described. These techniques, based on digital signal processing, are evaluated in a 64-QAM transceiver operating with a signal bandwidth of 2GHz.

The remainder of this article is structured as follows. Section II provides a description of the system architecture.

Section III introduces the NFS IQ imbalance issue, identifying and modeling the source of this impairment. The mitigation of the IQ imbalance impairment by digital signal processing at the receiver is also described in this section. In Section IV, a simulation model for the transceiver system, including the proposed mechanisms for reducing NFS IQ imbalance, is presented and analyzed. In Section V, the FS IQ imbalance issue is addressed and in Section VI the simulation results regarding this impairment are presented. Finally, some conclusions are drawn in Section VII.

II. System Architecture

In order to address new applications for the future backhauling networks, a point-to-point microwave link in the E-Band using a 64-QAM modulation with a signal bandwidth of 2GHz is considered. Fig. 1 shows the proposed transceiver (TRx) architecture for a point-to-point microwave link in the E-Band. As shown, the transmitter (Tx) front-end consists of an IQ up-converting modulator that up-converts the baseband I and Q channels to an intermediate frequency (IF). After combining the I and Q channels, the IF signal is up-converted by means of the millimeter-wave (mmW) mixer. Finally, the wideband mmW power amplifier (PA) is used to amplify and transmit the mmW signal. The receiver (Rx) front-end consists of a wideband Low Noise Amplifier (LNA), which receives and amplifies the signal at the E-Band. After the LNA, a first mixer down-converts the mmW signal to the same IF as in the Tx. This way, the same PLL can be re-used for the Tx and the Rx. Finally, an IQ demodulator down-converts the IF signal to 0-Hz.

This architecture presents a good balance between different design aspects, and it enables the minimization of the sampling frequency of the digital-to-analog (DAC) and analog-to-digital (ADC) converters. Nowadays, we can find commercial DACs and ADCs able to provide sampling rates close to 3Gsps, which is enough for practical implementation of the zero-second-IF architecture.

Due to the high channel bandwidth (higher than 2 GHz), the architecture depicted in Fig. 1 presents a good balance between the DAC and the ADC requirements and complexity on the transceiver. The use of other architectures, such as non-zero-second-IF would require very high performance ADCs or DACs, with sampling rates well above 4 Gsps to achieve a practical implementation of base-band and image rejection filters in the analog front-end. Other IF architectures, for example [7], relax the performance of the ADCs and DACs by using several sub-bands, but it is at the expense of increasing the complexity of the baseband and IF sections of the front-end of the transceiver.

However, the use of a zero-second-IF architecture presents well-known issues that should be addressed in order not to degrade the performance of the transceiver. This architecture is subject to corruption due to IQ imbalances at both the transmitter quadrature modulator and at the receiver demodulator . The resulting system performance degradation can be significant, especially for high-order modulation schemes [8].

III. Non-Frequency-selective IQ Imbalance

A. Imbalance analysis

The goal of the IQ modulator in Fig. 1 is to perform a frequency translation of the signal. That is, if the base-band input signal to the IQ modulator is

$$\tilde{s}(t) = s_I(t) + j s_Q(t), \tag{1}$$

where $s_I(t)$ is the signal in the I-datapath and $s_Q(t)$ is the signal in the Q-datapath, a perfect IQ modulation mixes the base-band input signal with

$$l_{\mathrm{tx}}(t) = e^{j\omega_{\mathrm{tx}}t} = \cos(\omega_{\mathrm{tx}}t) + j\sin(\omega_{\mathrm{tx}}t) \tag{2}$$

producing an output signal

$$s(t) = \mathrm{Re}\left[\tilde{s}(t) l_{\mathrm{tx}}(t)\right] = s_I(t)\cos(\omega_{\mathrm{tx}}t) - s_Q(t)\sin(\omega_{\mathrm{tx}}t). \tag{3}$$

However, when implementing an IQ modulator with actual electronic circuits, the signals produced by the local oscillator (LO) will present some difference in their amplitudes and will not have a phase difference of $\pi/2$. The effect of this imbalance can be modeled as the mixing of the base-band input signal with

$$l_{\mathrm{tx}}(t) = \cos(\omega_{\mathrm{tx}}t) + j g_{\mathrm{tx}} \sin(\omega_{\mathrm{tx}}t + \phi_{\mathrm{tx}}) \tag{4}$$

to yield the output signal

$$s(t) = (s_I(t) - g_{\mathrm{tx}}\sin(\phi_{\mathrm{tx}}) s_Q(t))\cos(\omega_{\mathrm{tx}}t) \tag{5a}$$

$$- s_Q(t) g_{\mathrm{tx}} \cos(\phi_{\mathrm{tx}})\sin(\omega_{\mathrm{tx}}t). \tag{5b}$$

In IQ imbalance analyses, it is common to rewrite the signal produced at the transmitter LO with the imbalance from equation (4) in the form of [9]

$$l_{\mathrm{tx}}(t) = C_1 e^{j\omega_{\mathrm{tx}}t} + C_2 e^{-j\omega_{\mathrm{tx}}t}, \tag{6}$$

with

$$C_1 = \frac{1 + g_{\mathrm{tx}} e^{j\phi_{\mathrm{tx}}}}{2} \tag{7a}$$

$$C_2 = \frac{1 - g_{\mathrm{tx}} e^{-j\phi_{\mathrm{tx}}}}{2} \tag{7b}$$

and the transmitted signal is

$$s(t) = \mathrm{Re}\left[\tilde{s}(t)\left(C_1 e^{j\omega_{\mathrm{tx}}t} + C_2 e^{-j\omega_{\mathrm{tx}}t}\right)\right]. \tag{8}$$

In (8), the desired term is the one multiplied by $e^{j\omega_{\mathrm{tx}}t}$ and the term multiplied by $e^{-j\omega_{\mathrm{tx}}t}$ is considered an undesired image. Equation (8) can be rewritten as

$$s(t) = \frac{1}{2}\left(C_1 \tilde{s}(t) e^{j\omega_{\mathrm{tx}}t} + C_1^* \tilde{s}^*(t) e^{-j\omega_{\mathrm{tx}}t}\right) \tag{9a}$$

$$+ \frac{1}{2}\left(C_2^* \tilde{s}^*(t) e^{j\omega_{\mathrm{tx}}t} + C_2 \tilde{s}(t) e^{-j\omega_{\mathrm{tx}}t}\right), \tag{9b}$$

where $(\cdot)^*$ denotes the complex conjugate.

Let $X(\omega)$ denote the Fourier Transform of a signal $x(t)$, then from (9) we have

$$S(\omega) = \frac{1}{2}\Big(C_1 \tilde{S}(\omega - \omega_{\mathrm{tx}}) + C_1^* \tilde{S}^*(\omega + \omega_{\mathrm{tx}}) \tag{10a}$$

$$+ C_2^* \tilde{S}^*(\omega - \omega_{\mathrm{tx}}) + C_2 \tilde{S}(\omega + \omega_{\mathrm{tx}})\Big). \tag{10b}$$

Fig. 2 illustrates the spectrum of $s(t)$. The first line in (10) is the desired term and the second line is an image that is an

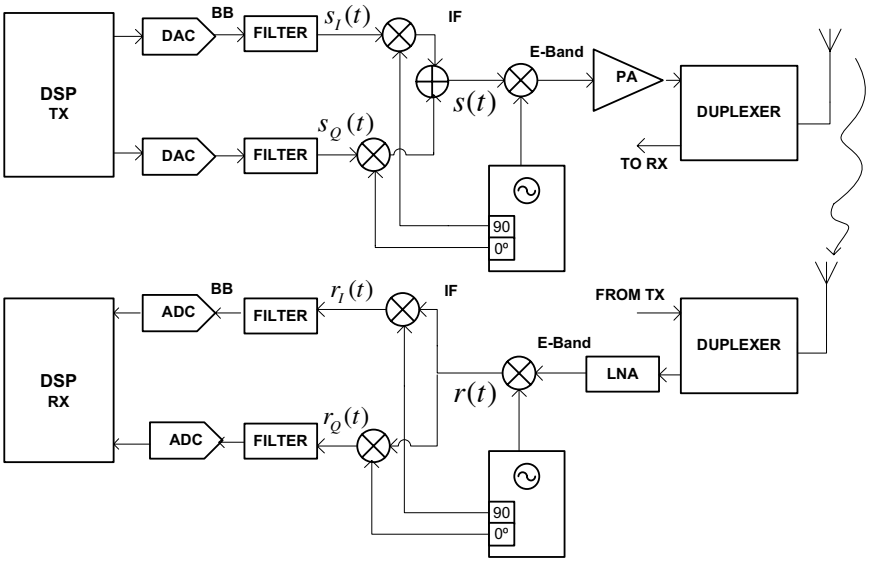

Fig. 1. Architecture of the transceiver.

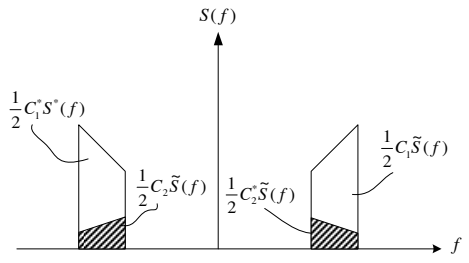

Fig. 2. Spectrum of $s(t)$ with imbalance.

alias of the desired signal. A measure of performance of the IQ modulator is the image rejection factor (IRR)

$$\mathrm{IRR}_{\mathrm{tx}} = \frac{|C_1|^2}{|C_2|^2} = \frac{1 + g_{\mathrm{tx}}^2 + 2g_{\mathrm{tx}}\cos(\phi_{\mathrm{tx}})}{1 + g_{\mathrm{tx}}^2 - 2g_{\mathrm{tx}}\cos(\phi_{\mathrm{tx}})}. \quad (11)$$

Similarly, the task of the Rx IQ demodulator in Fig. 1 is to mix the input signal with

$$l_{\mathrm{rx}}(t) = e^{-j\omega_{\mathrm{rx}}t} = \cos(\omega_{\mathrm{rx}}t) - j\sin(\omega_{\mathrm{rx}}t), \quad (12)$$

so that after low-pass filtering, the base-band equivalent of the signal in the frequency band of interest $\tilde{z}(t) = z_I(t) + jz_Q(t)$ is obtained. Note that $\tilde{z}(t)$ is the base-band equivalent that is referred to a carrier frequency ω_{rx}. The current implementation of the IQ demodulator will introduce similar imbalances to the actual implementation of the IQ modulator, which can be modeled as the mixing of $r(t)$ with

$$l_{\mathrm{rx}}(t) = \cos(\omega_{\mathrm{rx}}t) - jg_{\mathrm{rx}}\sin(\omega_{\mathrm{rx}}t + \phi_{\mathrm{rx}}). \quad (13)$$

The signal at the output of the IQ demodulator after low-pass filtering can be written as [9]

$$\tilde{r}(t) = r_I(t) + jr_Q(t) = K_1\tilde{z}(t) + K_2\tilde{z}^*(t) \quad (14)$$

with

$$K_1 = \frac{1 + g_{\mathrm{rx}}e^{-j\phi_{\mathrm{rx}}}}{2} \quad (15a)$$

$$K_2 = \frac{1 - g_{\mathrm{rx}}e^{j\phi_{\mathrm{rx}}}}{2}. \quad (15b)$$

In this case, the first term in the sum of (14) is the desired term and the second one is the image that aliases on the desired signal. The IRR for the IQ demodulator is defined as

$$\mathrm{IRR}_{\mathrm{rx}} = \frac{|K_1|^2}{|K_2|^2} = \frac{1 + g_{\mathrm{rx}}^2 + 2g_{\mathrm{rx}}\cos(\phi_{\mathrm{rx}})}{1 + g_{\mathrm{rx}}^2 - 2g_{\mathrm{rx}}\cos(\phi_{\mathrm{rx}})}. \quad (16)$$

Note that the above model for impairment affects to the whole information bearing signal in the same way. Although the model has been developed from the point of view of the local oscillators of the IQ modulator and demodulator, it can also be used to include the mean imbalances between the in-phase and quadrature datapaths.

In order to gain some insight, we assume enough linearity and proper filtering in the remaining stages of the transmitter and receiver analog chain and noise-less operation. Using (9), it can be seen that

$$\tilde{z}(t) = \left(C_1\tilde{s}(t) + C_2^*\tilde{s}^*(t)\right)e^{j(\Delta\omega t + \theta)} \quad (17)$$

where $\Delta\omega$ and θ account for the overall carrier frequency and phase offset between the transmitter and the receiver. Thus, we have

$$\tilde{r}(t) = K_1C_1\tilde{s}(t)e^{j(\Delta\omega t+\theta)} \quad (18a)$$

$$+ K_1C_2^*\tilde{s}^*(t)e^{j(\Delta\omega t+\theta)} \quad (18b)$$

$$+ K_2C_1^*\tilde{s}^*(t)e^{-j(\Delta\omega t+\theta)} \quad (18c)$$

$$+ K_2C_2\tilde{s}(t)e^{-j(\Delta\omega t+\theta)} \quad (18d)$$

The desired term in (18) is the one in the first line and the

terms in the second to fourth lines represent undesired images at the receiver due to transmitter and receiver IQ imbalances.

When $\Delta\omega = 0$, (18) simplifies to

$$\tilde{r}(t) = J_1\tilde{s}(t) + J_2\tilde{s}^*(t) \tag{19}$$

where J_1 and J_2 are constants given by

$$J_1 = K_1C_1e^{j\theta} + K_2C_2e^{-j\theta} \tag{20a}$$

$$J_2 = K_1C_2^*e^{j\theta} + K_2C_1^*e^{-j\theta}. \tag{20b}$$

Comparing (19) with (14), it can be concluded that when $\Delta\omega = 0$, the effect observed at the output of the receiver's IQ demodulator due to the IQ imbalance introduced at the transmitter is the same as the one due to an IQ imbalance introduced by the IQ demodulator. In a real transmission system there will be some carrier frequency offset between the transmitter and the receiver. However, the former observation suggests that the IQ imbalance introduced at the transmitter may be addressed after carrier frequency recovery using approaches designed to address the IQ imbalance introduced at the receiver.

B. Imbalance compensation

1) Tx IQ Imbalance Compensation: Using (1) and (3) with $\tilde{s}'(t) = s'_I(t) + js'_Q(t)$ denoting the equivalent baseband signal of the Tx IQ distorted signal $s(t)$ with respect to the transmitter carrier frequency ω_{tx}, we can derive the following matrix equation for Tx IQ imbalance distortion:

$$\begin{bmatrix} s'_I(t) \\ s'_Q(t) \end{bmatrix} = \begin{bmatrix} 1 & -g_{tx}\sin(\phi_{tx}) \\ 0 & g_{tx}\cos(\phi_{tx}) \end{bmatrix} \begin{bmatrix} s_I(t) \\ s_Q(t) \end{bmatrix}. \tag{21}$$

If the matrix in (21) is invertible ($g_{tx} \neq 0$ and $\phi_{tx} \neq \pm\pi/2$), which is the case in practical cases, the Tx NFS IQ compensation can ideally be achieved by performing a digital predistortion based on the inverse operation. In this case, we feed the IQ modulator with the predistorted signal $\varsigma(t) = \varsigma_I(t) + j\varsigma_Q(t)$, which is obtained as

$$\begin{bmatrix} \varsigma_I(t) \\ \varsigma_Q(t) \end{bmatrix} = \begin{bmatrix} 1 & \tan(\phi_{tx}) \\ 0 & 1/(g_{tx}\cos(\phi_{tx})) \end{bmatrix} \begin{bmatrix} s_I(t) \\ s_Q(t) \end{bmatrix}. \tag{22}$$

Compensation by inverse transformation requires knowledge of the gain and phase imbalance values, g_{tx} and ϕ_{rx}.

Techniques for compensating the IQ imbalance at the transmitter that have been proposed in the literature use tones as test signals (e.g., [10], [11], [12], [13]) or even from random data (e.g., [11], [14]). Compensating by using test tones is very powerful and can be used for initial calibration. During normal full-duplex operation of the transceiver, IQ imbalance compensation from the random transmitted data would be preferred. All these techniques of compensation require additional circuitry (including an extra ADC) at the transmitter to feed back measurements performed in the analog front-end.

Under certain conditions the Tx IQ imbalance can also be compensated in the receiver (see [9]). For this to be possible, the spectral images caused by the Tx IQ imbalance have to be emitted and a carrier frequency offset between transmitter and receiver is required to be able to decouple the Tx and Rx IQ imbalance effects in the receiver [15], [16]. As these conditions are fulfilled in the analyzed system, receiver-based compensation for both frequency-independent and frequency-selective Tx IQ imbalance is the approach investigated in this article, because it does not require any additional circuitry in the analog front-end of the transceiver and all the compensation can be performed by digital signal processing.

2) Rx IQ Imbalance Compensation: The down-converted complex-valued base-band signal $\tilde{r}(t)$ can be written as a function of $\tilde{z}(t)$ using the following matrix equation

$$\begin{bmatrix} r_I(t) \\ r_Q(t) \end{bmatrix} = \begin{bmatrix} 1 & 0 \\ -g_{rx}\sin(\phi_{rx}) & g_{rx}\cos(\phi_{rx}) \end{bmatrix} \begin{bmatrix} z_I(t) \\ z_Q(t) \end{bmatrix}. \tag{23}$$

In case the matrix in (23) is invertible ($g_{rx} \neq 0$ and $\phi_{rx} \neq \pm\pi/2$), which is the case in practical cases, the Rx IQ imbalance can be ideally compensated by performing the inverse operation

$$\begin{bmatrix} \alpha_I(t) \\ \alpha_Q(t) \end{bmatrix} = \begin{bmatrix} 1 & 0 \\ \tan(\phi_{rx}) & 1/(g_{rx}\cos(\phi_{rx})) \end{bmatrix} \begin{bmatrix} z'_I(t) \\ z'_Q(t) \end{bmatrix}, \tag{24}$$

where $\alpha(t) = \alpha_I(t) + j\alpha_Q(t)$ is the output of the Rx IQ imbalance compensator and ideally would yield the desired baseband signal $\tilde{z}(t)$. Compensation by inverse transformation requires knowledge of the gain and phase imbalance values g_{rx} and ϕ_{rx}, which can be derived by using statistics and the correlation properties of the I and Q signals as proposed in [17].

IV. NFS IQ Imbalance Simulation Results

A. System Model

The system model depicted in Fig. 3 constitutes the basis for the simulations of the impact of Tx and Rx IQ imbalance impairments and their respective compensation algorithms on the performance of the E-band transceiver.

Random data information is generated as a sequence of IQ symbols, *D*, by using a 64QAM mapper. *D* is then filtered through an appropriate root-raised-cosine (RRC) filter to create a pulse-shaped base-band signal, $x(t)$. The Tx Baseband Filtering and Mixing models the data processing as shown in Fig. 1. There is the option of employing Tx IQ predistortion to mitigate the NFS Tx IQ imbalance, but for the purposes of this paper, this block will be deactivated.

Considering an additive white Gaussian noise (AWGN) channel, the signal $\tilde{z}$ at the output of the channel model is given by:

$$\tilde{z}(t) = \tilde{s}(t) \cdot \mathrm{e}^{j2\pi ft} + n(t), \tag{25}$$

where $\tilde{z}(t)$ is the low-pass equivalent of the transmitted signal, $\tilde{s}(t)$ is the transmitted signal and $\mathrm{e}^{j2\pi ft}$ represents the carrier frequency offset (CFO), with f as the frequency offset. This CFO is produced by the difference between the oscillators of the transmitter and receiver. Finally, $n(t)$ corresponds to a complex-valued white Gaussian noise process.

On the receiver side, the Rx Baseband Filtering and Mixing models the receiver analog front-end structure shown in Fig. 1, including Rx IQ imbalance. NFS IQ Imbalance Compensation

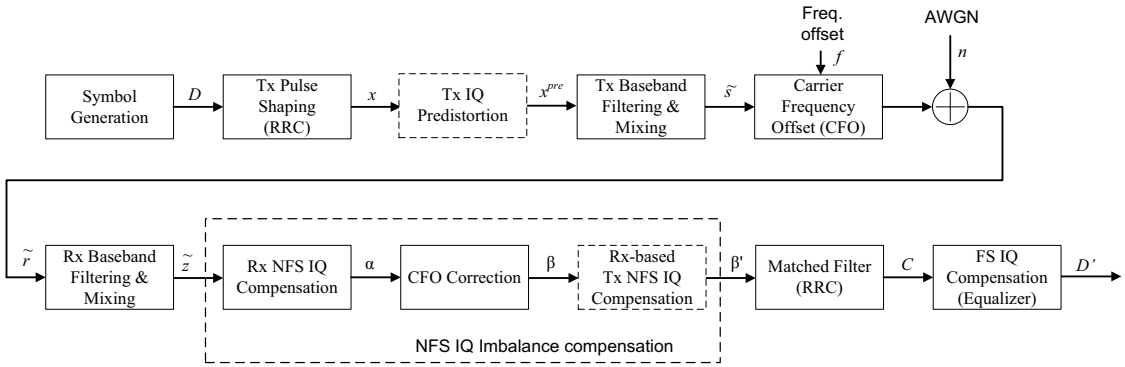

Fig. 3. System Model for IQ Imbalance Simulations.

is performed prior to matched filtering by following a multi-stage approach that compensates for both Tx and Rx IQ Imbalance:

1) The first stage compensates for the Rx NFS IQ imbalance based on the algorithms in Section III-B.
2) A CFO correction stage ideally compensates the CFO introduced by the difference of the transmitter and receiver, using the relation $\beta(t) = \alpha(t) \cdot \mathrm{e}^{-i2\pi ft}$
3) A third stage performs Tx NFS IQ imbalance compensation prior to the matched ltering by re-applying the algorithms in Section III-B .

After NFS IQ Imbalance Compensation the signal is filtered with a matched RRC filter. The equalizer used to compensate the FS IQ imbalance is ignored in this section (i.e., $D' = C$). The received symbols *D'* are compared with the transmitted symbols *D* to quantify the performance of the whole system.

B. NFS IQ Imbalance results

Fig. 4(a) illustrates the effect of NFS IQ imbalance. For illustration purposes, a noiseless transmission is considered. Crosses correspond to the constellation where perfect transmission takes places, and the dots correspond to a transmission with IQ imbalances both at transmitter and receiver, assuming zero carrier frequency offset. The IQ imbalances considered were 0.5 dB and 3 degrees in gain and phase, respectively, in the transmitter and 1 dB and 3 degrees in gain and phase, respectively, in the receiver. The signs of the imbalances were selected in the transmitter and the receiver so that they combine in the worst possible distortion. Fig. 4(b) shows the constellation at the receiver when the NFS IQ imbalance compensation is active. It can be seen that the NFS IQ imbalance compensation approach is able to remove the distortion effect on the constellation.

Fig. 5 shows the impact of the NFS IQ imbalance in the performance of the transceiver. The curve labeled *'without NFS IQ'* is the performance of the transceiver when there is no IQ imbalance. The curve labeled *'NFS IQ'* is the performance of the transceiver with IQ imbalance at both transmitter and receiver. The curve labeled *'NFS IQ with comp'* is the

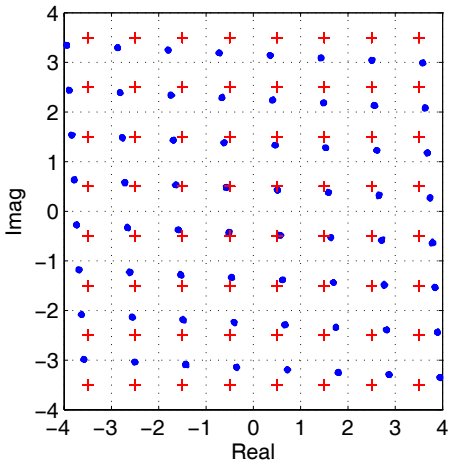

(a) Without compensation

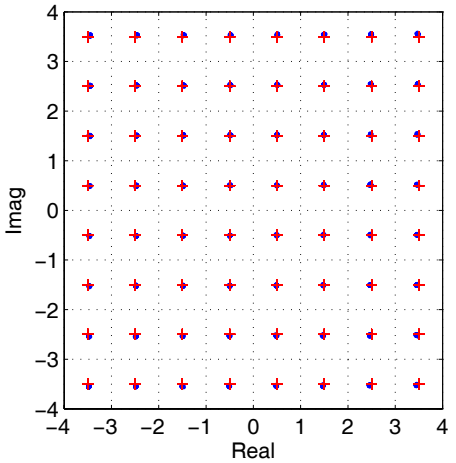

(b) With compensation

Fig. 4. NFS IQ imbalance

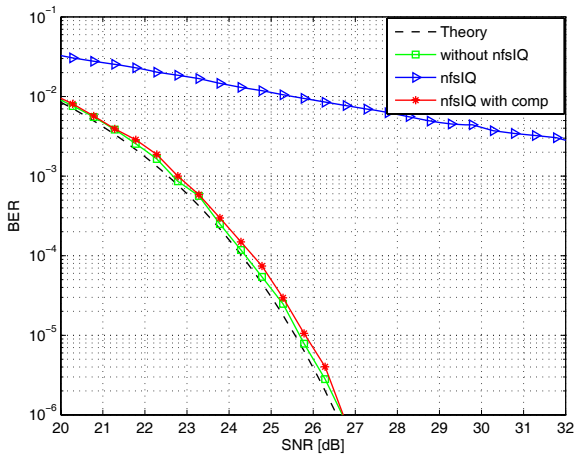

Fig. 5. System performance in the presence of NFS IQ imbalance.

performance when the IQ imbalance compensation is active. The NFS IQ imbalance compensation is able to reduce the losses to a few tenths of a dB.

Fig. 6(a) illustrates the effect of NFS IQ imbalance when there is a residual carrier frequency offset equal to $\Delta\omega = 2\pi \cdot 5 \cdot 10^{-6}/T$ after the CFO correction in Fig. 3, where T is the symbol period. For proper symbol detection and Bit Error Rate(BER) estimation, the residual carrier frequency offset was compensated in the simulations at the input of the receiver's matched-filter. The figure shows the corrected constellations after the final residual carrier frequency offset compensation. The transmitter's IQ imbalance manifests itself as rotations of the constellation around the distorted constellation due to the receiver's IQ imbalance.

Fig. 6(b) shows the constellation when the IQ compensation algorithms are active for the same residual carrier frequency offset. It can be seen that the distortion of the constellation has been reduced despite some residual carrier frequency offset.

Fig. 7 shows the impact of the residual carrier frequency offset on the performance of the NFS IQ imbalance compensation approach presented in Section III-B. The different curves correspond to different values of the normalized residual carrier frequency offset $\Delta\omega T/(2\pi)$. It can be seen that a very accurate carrier frequency offset correction is needed for proper compensation of the transmitter IQ imbalance with residual CFO below $\Delta\omega T/(2\pi) = 5 \cdot 10^{-6}$, which can be achieved via application of state of the art coarse and fine frequency synchronization algorithms [18].

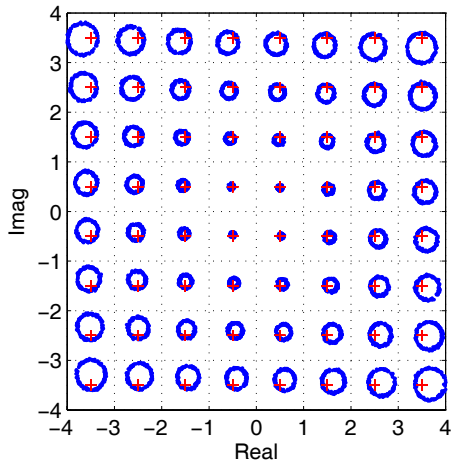

(a) Without compensation

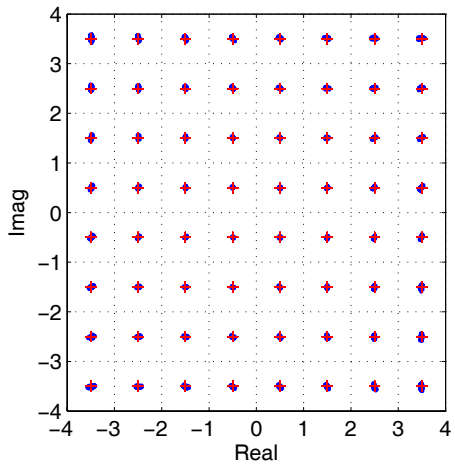

(b) With compensation

Fig. 6. NFS IQ imbalance with normalized residual carrier frequency offset $\Delta\omega T/(2\pi) = 5 \cdot 10^{-6}$.

V. Frequency-selective IQ Imbalance

A. Imbalance analysis and models

The above analysis considers that the imbalance is constant with frequency, and thus we talk about non-frequency-selective IQ imbalance. Nevertheless, the elements placed in the I-datapath and Q-datapath present dispersion in their parameters. Therefore, there will always be a difference between the performance of the components placed in the I-datapath and the components placed in the Q-datapath. These dispersions can contribute to non-frequency-selective distortion, and likewise to impairment due to the LOs, or to frequency-selective distortion. For instance, Fig. 8 compares the frequency responses (magnitude and phase) of the designed passive baseband filters by considering typical values for the fabrication tolerances of their components. L0C0 is the nominal case. LpCp is the corner where inductors and capacitances have their maximum value. LmCm is the corner where inductors and capacitors have their minimum value. Fig. 9 shows the difference between the two extreme corners. This kind of mismatch between the components in the I and Q datapaths is a frequency-selective IQ imbalance.

Fig. 10 shows the BER performance of the system obtained from the model that compensates the non-frequency-selective IQ imbalance, but does not correct the frequency-selective mismatch. The FS IQ imbalance is considered at both the transmitter and the receiver sides of the transceiver. The curve labeled *'IbbfiltL0C0, QbbfiltL0C0'* represents the nominal

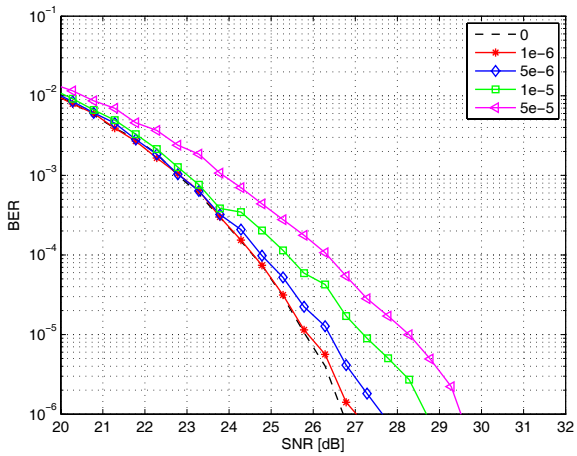

Fig. 7. Performance of NFS IQ imbalance compensation approach for different values of $\Delta\omega T/(2\pi)$.

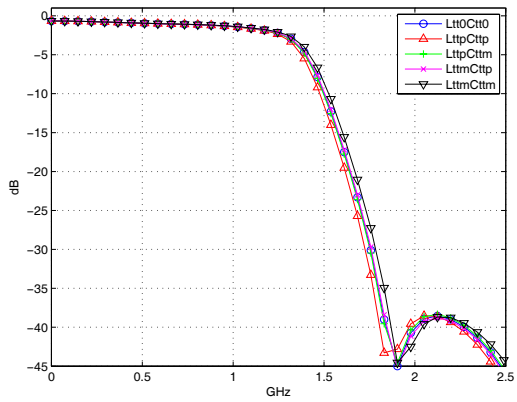

(a) Magnitude variation

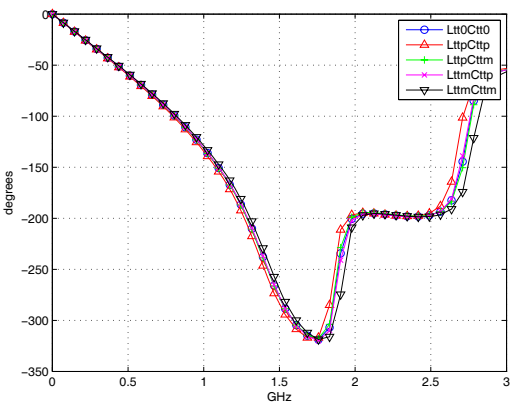

(b) Phase variation

Fig. 8. Variation of frequency response of base-band filters.

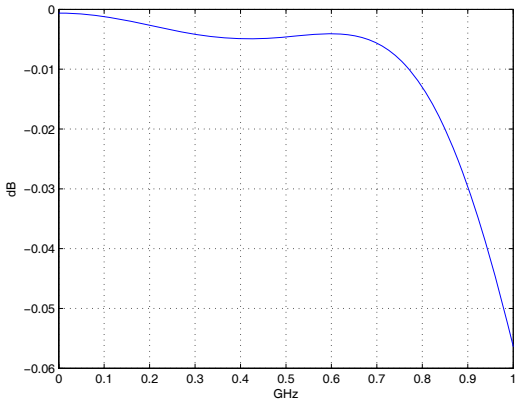

(a) Magnitude variation

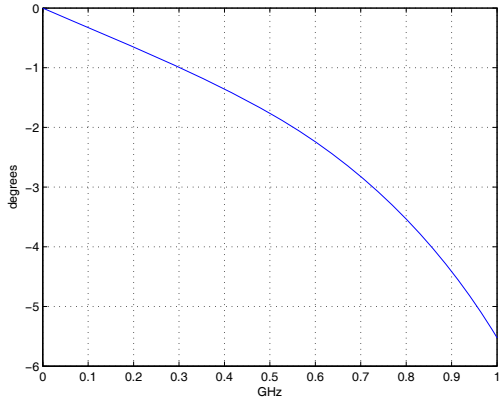

(b) Phase variation

Fig. 9. Frequency response of base-band filters in extreme corners.

case, i.e., the case without FS IQ imbalance. The curve labeled *'IbbfiltLpCp, QbbfiltLmCm'* is the case in which an LpCp base-band filter has been considered in the I-datapath and an LmCm base-band filter has been chosen for the Q-datapath in the transmitter and the receiver. From the BER performance it can be concluded that the loss due to FS IQ imbalance significantly degrades the performance of the system, since for a BER of 10^{-6} in the case of uncoded 64QAM, a loss of more than 2dB is shown.

In the literature more articles focusing on the modeling and compensation of non-frequency-selective IQ imbalance can be found. However, this approach has become insufficient as the use of wider bandwidth signals has become more prevalent. Therefore, as we can conclude from Fig. 10, for wide bandwidth signals the above technique for compensating for the non-frequency-selective IQ imbalance is generally insufficient, as the IQ imbalance is likely to be frequency-dependent.

The frequency-dependent imbalances of the quadrature mixing front-end may include contributions from the DAC/ADC, low-pass filters, as well as the signal paths themselves. To formally analyze the detrimental effect of these IQ mismatches,

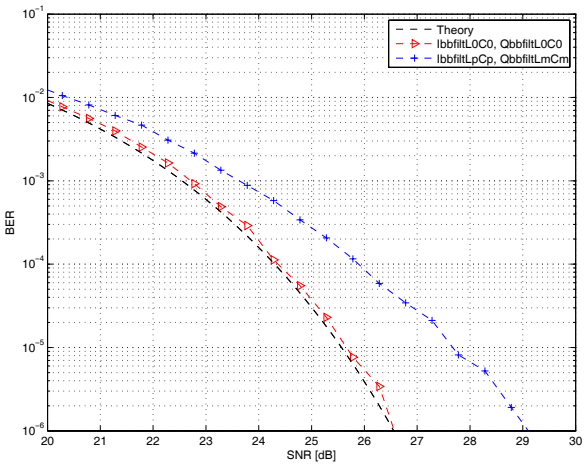

Fig. 10. System performance in the presence of FS IQ imbalance..

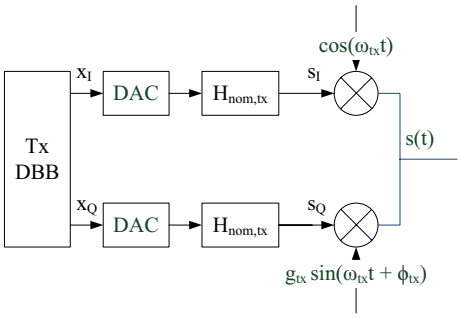

Fig. 11. Tx IQ Imbalance Model.

the combined effect can simply be modeled as a pair of two imbalanced base-band filters. The models depicted in Fig. 11 and Fig. 12 have been devised as a basis for the development of algorithms for Tx and Rx IQ imbalance compensation.

For Tx IQ imbalance in Fig. 11 the filters $H_{nom,tx}(f)$ are assumed to be ideal low-pass filters with $H_{nom,tx}(f) = 1$ for $|f| \leq B_{tx}/2$ and $H_{nom,tx}(f) = 0$ for $|f| > B_{tx}/2$, where B_{tx} is the bandwidth of the transmitted signal of interest. In analyzing NFS IQ imbalance, these filters are assumed to be virtually ineffective. The filters $H_{I,tx}(f)$ and $H_{Q,tx}(f)$ are modeling frequency-dependent or frequency-selective mismatches between the I and Q path, as shown in Fig. 8 and Fig. 9.

The corresponding model for Rx IQ imbalance is depicted in Fig. 12 (see also [19], [6]). The filters $H_{nom,rx}(f)$ are assumed to be ideal low-pass filters with $H_{nom,rx}(f) = 1$ for $|f| \leq B_{rx}/2$ and $H_{nom,rx}(f) = 0$ for $|f| > B_{rx}/2$, where B_{rx} is the bandwidth of the received signal of interest. Similar to the TX IQ imbalance model in Fig. 11, the filters $H_{I,rx}(f)$ and $H_{Q,rx}(f)$ are modeling frequency-dependent or frequency-selective mismatches between the I and Q paths.

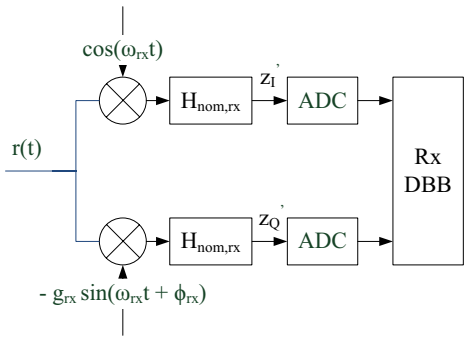

Fig. 12. Rx IQ Imbalance Model.

B. Frequency-Selective IQ Imbalance Compensation

Methods for compensating Rx FS IQ imbalance are reported in [6], [5]. In [6], an adaptive filter is employed to perform interference cancellation. In [5], a simplified compensation method, based on mean values of the FS IQ imbalance, is presented. However, this method assumes prior knowledge of the mean values over frequency for the frequency-selective part of the amplitude and phase imbalances.

In this article, a linear adaptive equalizer (LAE) is deployed for the FS IQ imbalance compensation as shown in the system model in Fig. 3. In addition to NFS IQ Imbalance compensation analyzed in Section IV-B, the LAE is activated as the final stage in performing compensation of FS IQ imbalance after matched filtering. The LAE performs linear filtering of the Matched Filter output as defined by (26). The LAE facilitates FS IQ compensation without prior knowledge of the frequency responses of frequency-selective amplitude and phase imbalances. The L coefficients w_i in (26) are calculated and adapted based on known symbol sequences in the data stream using the Least Mean Square (LMS) algorithm. For the following simulations an equalizer length of $L = 15$ is used.

$$D'[k] = \sum_{i=0}^{L-1} w_i C[k-i]. \tag{26}$$

The system performance in terms of FS IQ Imbalance distortion is evaluated in terms of residual carrier-to-distortion ratio after the LAE is defined by the relation

$$\frac{C}{ISI} = \frac{E\left\{|D|^2\right\}}{E\left\{|D-D'|^2\right\}}, \tag{27}$$

where $E\left\{|D|^2\right\}$ is the energy of the transmitted signal D and $E\left\{|D-D'|^2\right\}$ denotes the energy of the received signal error, i.e., distortion caused by residual inter-symbol-interference (ISI) and image interference. Simulation results are provided in Section VI.

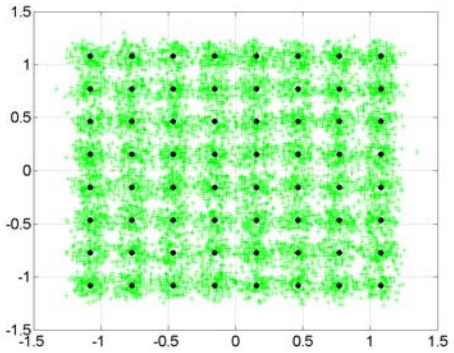

(a) Without equalizer

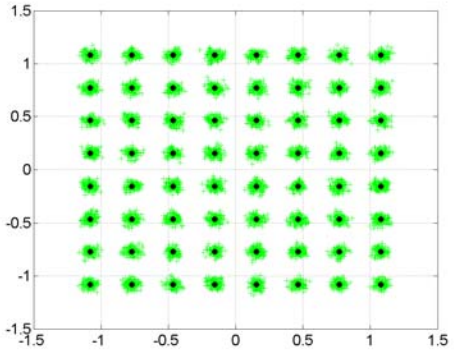

(b) With equalizer

Fig. 13. Signal Constellations (64QAM)

VI. FS IQ Imbalance Simulation Results

Fig. 13 shows the constellation diagrams for 64QAM after the RRC matched filter and the equalizer, respectively. The circles in the diagrams correspond to the ideal constellation points. When comparing Fig. 13(a) with Fig. 13(b) the reduction in residual distortion achieved by the equalizer can be observed.

For a BER of 10^{-6} in the case of uncoded 64QAM a $C/(I+ISI) = 26.54\,dB$ is required at the input to the demapper, which corresponds to the output of equalizer *D'*. Table I summarizes the performance for different transmit and receive filter pairs based on the frequency responses shown in Fig. 8 and Fig. 9. Simulations 1 to 3 have been run with identical filters for both quadrature components in the transmitter and receiver. The residual ISI is in the range of 38 dB. Simulations 4 to 9 have been run with imbalanced quadrature filters. The FS IQ imbalance, i.e., the difference between frequency responses, is most severe in simulations 4 and 5, where the corner cases LpCp and LmCm for the tolerances concerning the frequency responses have been used. The residual ISI after the equalizer is reduced below levels where 64QAM can be decoded. For less severe filter imbalances, as in simulations 6 to 9, the residual ISI is about 4 to 5 dB better.

TABLE I
FS IQ Imb. Performance

	$H_{I,tx}(f)$	$H_{Q,tx}(f)$	$H_{I,rx}(f)$	$H_{Q,rx}(f)$	C/ISI [dB]
1	L0C0	L0C0	L0C0	L0C0	38.5
2	LpCp	LpCp	LpCp	LpCp	38.4
3	LmCm	LmCm	LmCm	LmCm	37.8
4	LpCp	LmCm	LpCp	LmCm	27.1
5	LmCm	LpCp	LmCm	LpCp	29.0
6	LpCp	L0C0	LpCp	L0C0	31.9
7	L0C0	LpCp	L0C0	LpCp	34.6
8	LmCm	L0C0	LmCm	L0C0	34.7
9	L0C0	LmCm	L0C0	LmCm	34.6

VII. Conclusion

In this article, a theoretical analysis of the IQ imbalance in a heterodyne transceiver with zero-second-IF has been presented. Digital signal processing at the receiver has been evaluated based on a multi-stage approach for the compensation of both transmitter and receiver IQ imbalance, as well as carrier frequency offset.

Simulation results were presented for a zero-second-IF transceiver using 64-QAM with a signal bandwidth of 2GHz. For NFS IQ imbalance, the simulation results show that receiver-based Tx IQ imbalance compensation can be achieved with negligible degradation in overall system performance. This is achieved when accurate frequency synchronization is performed in the receiver such that the residual carrier frequency offset is reduced below specified limits. For FS IQ imbalance, simulation results have demonstrated that FS IQ imbalance can be mitigated by a receiver-based compensation concept based on linear equalization.

Acknowledgment

The research leading to these results has received funding from the European Community's FP7/2007-2013 Framework Programme under grant agreement no. 317957. Consortium: CEIT, Fraunhofer IIS, Alcatel-Lucent, CEA-Leti, IXYS, Silicon Radar, ST, Sivers IMA, OTE.

References

[1] A. Rezola, J. Sevillano, R. Berenguer, I.Velez, M. Leyh, M. Lorenzo, and A. Vargas, "Non-frequency-selective i/q imbalance in zero-if transceivers for wide-band mmw links," in *The Tenth International Conference on Wireless and Mobile Communications ICWMC*, 2014, pp. 136–141.

[2] *Fixed Radio Systems; Characteristics and requirements for point-to-point equipment and antennas; Part 1: Overview and system-independent common characteristics*, ETSI EN 302 217-1, Sept. 2012.

[3] *Fixed Radio Systems; Characteristics and requirements for point-to-point equipment and antennas; Part 2-2: Digital systems operating in frequency bands where frequency co-ordination is applied; Harmonized EN covering the essential requirements of article 3.2 of the R&TTE Directive*, ETSI EN 302 217-2-2, Sept. 2012.

[4] G. Fettweis, M. Lohning, D. Petrovic, M. Windisch, P. Zillmann, and W. Rave, "Dirty RF: a new paradigm," in *Personal, Indoor and Mobile Radio Communications, 2005. PIMRC 2005. IEEE 16th International Symposium on*, vol. 4, 2005, pp. 2347–2355 Vol. 4.

[5] M. Mailand, R. Richter, and H.-J. Jentschel, "IQ-imbalance and its compensation for non-ideal analog receivers comprising frequency-selective components," *Advances in Radio Science*, vol. 4, pp. 189–195, Sept. 2006.

[6] M. Valkama, M. Renfors, and V. Koivunen, "Compensation of frequency-selective i/q imbalances in wideband receivers: models and algorithms," in *Wireless Communications, 2001. (SPAWC '01). 2001 IEEE Third Workshop on Signal Processing Advances in*, 2001, pp. 42–45.

[7] V. Dyadyuk, J. Bunton, J. Pathikulangara, R. Kendall, O. Sevimli, L. Stokes, and D. Abbott, "A multigigabit millimeter-wave communication system with improved spectral efficiency," *Microwave Theory and Techniques, IEEE Transactions on*, vol. 55, no. 12, pp. 2813–2821, Dec 2007.

[8] B. Razavi, "Design considerations for direct-conversion receivers," *Circuits and Systems II: Analog and Digital Signal Processing, IEEE Transactions on*, vol. 44, no. 6, pp. 428–435, Jun 1997.

[9] L. Antilla, "Digital Front-End Processing with Widely-Linear Signal Models in Radio Devices," Ph.D. dissertation, Tampere University of Technology, 2011.

[10] J. Cavers and M. Liao, "Adaptive compensation for imbalance and offset losses in direct conversion transceivers," *Vehicular Technology, IEEE Transactions on*, vol. 42, no. 4, pp. 581–588, Nov 1993.

[11] J. Cavers, "New methods for adaptation of quadrature modulators and demodulators in amplifier linearization circuits," *Vehicular Technology, IEEE Transactions on*, vol. 46, no. 3, pp. 707–716, Aug 1997.

[12] A. Nassery, S. Byregowda, S. Ozev, M. Verhelst, and M. Slamani, "Built-in-self test of transmitter i/q mismatch using self-mixing envelope detector," in *VLSI Test Symposium (VTS), 2012 IEEE 30th*, 2012, pp. 56–61.

[13] S. D'souza, F. Hsiao, A. Tang, S.-W. Tam, R. Berenguer, and M.-C. Chang, "A 10-bit 2-gs/s dac-ddfs-iq-controller baseband enabling a self-healing 60-ghz radio-on-chip," *Circuits and Systems II: Express Briefs, IEEE Transactions on*, vol. 60, no. 8, pp. 457–461, Aug 2013.

[14] X. Huang and M. Caron, "Efficient transmitter self-calibration and amplifier linearization techniques," in *Circuits and Systems, 2007. ISCAS 2007. IEEE International Symposium on*, 2007, pp. 265–268.

[15] P. Rykaczewski and F. Jondral, "Blind i/q imbalance compensation in multipath environments," in *Circuits and Systems, 2007. ISCAS 2007. IEEE International Symposium on*, May 2007, pp. 29–32.

[16] J. de Witt and G.-J. van Rooyen, "A blind i/q imbalance compensation technique for direct-conversion digital radio transceivers," *Vehicular Technology, IEEE Transactions on*, vol. 58, no. 4, pp. 2077–2082, May 2009.

[17] H.-J. Jentschel, "Direct conversion receivers - expectations and experiences," in *RF Front End Architectures, IEEE MTT-S 2000, Boston, Workshop*, June 2000.

[18] H. Meyr, M. Moeneclaey, and S. A. Fechtel, *Digital Communication Receivers*. Wiley, 1998.

[19] M. Valkama, M. Renfors, and V. Koivunen, "Advanced methods for i/q imbalance compensation in communication receivers," *Signal Processing, IEEE Transactions on*, vol. 49, no. 10, pp. 2335–2344, Oct 2001.